Biomass Conversion and Biorefinery (2024) 14:16843–16856
https://doi.org/10.1007/s13399-022-03709-1

ORIGINAL ARTICLE

# Green synthesis of nanostructured zinc oxide by *Ocimum tenuiflorum* extract: characterization, adsorption modeling, cytotoxic screening, and metal ions adsorption applications

**Rehab M. I. Elsamra[1] · Mamdouh S. Masoud[1] · Alyaa A. Zidan[1,2] · Gehan M. El Zokm[2] · Mohamed A. Okbah[2]**

Received: 30 October 2022 / Revised: 19 December 2022 / Accepted: 22 December 2022 / Published online: 9 January 2023
© The Author(s) 2023

## Abstract

Nano-ZnO was synthesized by the reduction of Zn $(CH_3COO)_2.2H_2O$ salt using the extract of *Ocimum tenuiflorum* leaves. The generated ZnO NPs were characterized by FT-IR, XRD, SEM, and EDX techniques. FT-IR results approved the characteristic peaks, the formation of ZnO bonds, and the morphology changes after the adsorption of $Cd^{2+}$ and $Pb^{2+}$ from solutions. The outlined data of the XRD pointed to the formation of a hexagonal wurtzite structure. SEM images showed the spherical nature of the synthesized particles with an average diameter of 19 nm. Moreover, the best conditions for the adsorption of $Cd^{2+}$ and $Pb^{2+}$ by ZnO NPs were evaluated and fitted to isotherm and kinetic models. Short contact time of ~ 20 min and a small sorbent dosage of 40 mg were sufficient conditions for attaining maximum $Pb^{2+}$ adsorption capacity. Based on the modeling parameters, the adsorption follows pseudo-second-order kinetics where ZnO and metal ions are involved in the rate-determining step. Two important applications were thoroughly studied. The nanoparticles significantly removed $Pb^{2+}$ and $Cd^{2+}$ contaminants from real environmental water samples collected from different locations in Egypt. Additionally, the cytotoxic activity results provided perfect evidence for the higher efficacy of the synthesized ZnO NPs as an anticancer agent against Panc-1, PC-3, and CACO-2 cell lines with $IC_{50}$ of 1.70, 3.67, and 5.70 $\mu gml^{-1}$, respectively, compared to cisplatin ($IC_{50}$ = 3.57, 5.09, and 7.75 $\mu gml^{-1}$). Furthermore, a low cytotoxic effect was observed on the normal human lung cell line (MRC-5, $IC_{50}$ = 22.40 $\mu gml^{-1}$). The data can be used as a preliminary study for anticancer drug design after further clinical investigations.

**Keywords** ZnO NPs · Green synthesis · Metal ions adsorption · Isotherms · Anticancer activity

**Highlights**
- Green synthesis of ZnO NPs utilizing the extract of *Ocimum Tenuiflorum* leaves.
- Characterization of the yielded nanoparticles by FT-IR, XRD, X-ray, and SEM techniques.
- Optimum adsorption conditions for the elimination of $Cd^{2+}$ and $Pb^{2+}$ from solutions and adsorption isotherms.
- High efficiency of removal of $Cd^{2+}$ and $Pb^{2+}$ from real environmental water samples.
- Evidence for high cytotoxic activity of the synthesized ZnO NPs against Panc-1, PC-3, and CACO-2 cell lines compared to cisplatin.

## 1 Introduction

Nanoparticle-sized materials have been the platform of intense investigations for their valuable applications in almost all fields of technology [1–4]. Among the key nanoparticle materials with successful practices is the metal oxide nanosized such as ZnO NPs, which has been proposed as a photocatalytic substance with a wide bandgap of 3.37 eV and an exciton-binding energy of 60 meV [5, 6].

✉ Rehab M. I. Elsamra
rehab_elsamra@alexu.edu.eg

Mamdouh S. Masoud
Mamdouh.saad@alexu.edu.eg

Alyaa A. Zidan
aliaa.ali47@yahoo.com

Gehan M. El Zokm
gehanelzokm@yahoo.com

Mohamed A. Okbah
m_okbah@yahoo.com

[1] Chemistry Department, Faculty of Science, Alexandria University, P.O. Box 426, Alexandria 21321, Egypt

[2] National Institute of Oceanography and Fisheries, NIOF, Cairo, Egypt

ZnO NPs are effective adsorbates [7], coating elements for cellulose fibers [8], and magnetic materials used in information storage devices [9]. Besides, the small size and hence great surface area and surface energy of ZnO NPs allow different pharmacological and biomedical activities as antibacterial, fungicidal, and anticancer agents [10–13]. ZnO NPs showed high cytotoxic activity on different cell lines [14, 15], where the nanoparticles cause rounding of cells and reduction in the nuclear volume leading to nuclei fragmentation and release of apoptotic bodies [12]. It is well established that green synthesis of nanoparticles offers an economical preparation method and yields low toxic nanoproducts with versatile applications [16–18]. Seaweeds, microorganisms, and plant extracts are examples of biomaterials that cause metal reduction leading to nanoparticle formation [19, 20]. Another feature of ZnO NPs that attracted many research works is their superior effect as heavy metal removal in the water treatment process [7, 21–23]. Generally, the existence of heavy metal ions in water streams is a global problem. Some metal ions as $Pb^{2+}$ and $Cd^{2+}$ are lethal to the environment even in trace concentrations due to their high toxicity, relative bioavailability, and low degradability that results in a high tendency of accumulation. Many health problems arise from the intake of water contaminated by $Pb^{2+}$ and $Cd^{2+}$ [24, 25]. Due to the rapid and growing industrialization which increases the mass of annual discharge of metal ions to the water systems, there is a continuous need for developing methods for treating water from such contaminants. Various adsorption substances are efficient in capturing heavy metals from solutions such as humic acid, zeolite [26], and chitosan [27]. In consideration of the pertinent applications of ZnO NPs, the current work is our contribution to the green synthesis of ZnO NPs employing plant extract. The yielded nanoparticles were screened for their biological activities. Furthermore, the adsorption capacity of the synthesized ZnO NPs was assessed by removing $Pb^{2+}$ and $Cd^{2+}$ from environmental water samples collected from fresh, brackish, and seawater from different locations in Alexandria, Egypt.

## 2 Experimental

### 2.1 Chemicals

The chemicals utilized are of high analytical grades (Merck) and were used without further purification. Stock solutions of cadmium acetate dihydrate (purity ≥ 98%) and lead nitrate (purity ≥ 99%) were prepared in deionized double-distilled water and used as sources of the investigated ions Cd(II) and Pb(II) respectively. Zinc acetate dihydrate ($Zn(CH_3COO)_2.2H_2O$, purity ≥ 98%) was used for the synthesis of ZnO nanoparticles. Also, analytical grade sodium acetate anhydrite (1 M) and hydrochloric acid (1 M) were used to prepare the buffering system of different pH values (pH = 2–7). The interfering ion solutions were prepared by dissolving 0.1 g of the salts; KCl, NaCl, $MgSO_4$, $KNO_3$, $NaCO_3$, and $CaCO_3$ in 25 ml of deionized water. The solution was then mixed with the investigated metal ion solutions under their specific optimum adsorption conditions which were determined in separate experiments.

### 2.2 Instruments

Different techniques were used in the characterization of ZnO NPs and their adsorption capacity. The pH value of water samples was measured by calibrated Electrochemistry Analyzer pH-meter (JENWAY 3505). The infrared spectrum was recorded in the range 400–4000 $cm^{-1}$ with the BRUKER TENSOR 37 FT-IR spectrophotometer. The surface topography and particle size of the synthesized ZnO NPs were scanned by a scanning electron microscope (SEM, Model: JEOL-JSMIT 200). The nanoparticles sizes and shapes were further detected by transmission electron microscope (TEM, Model: JSM-1400 PLUS). Elemental analysis of the samples was performed by energy-dispersive X-ray emission spectroscopy, EDX. Also, the phase identification and the lattice spacing (*d*) in ZnO NPs sample were detected by the X-ray diffractometers using Cu Kα as a radiation source of wavelength ($\lambda = 1.5406$ Å) at a current of 30 mA with 40 kV. The data were scanned at $2\theta$ in the range of 0 to 70°. The concentration of $Pb^{2+}$ and $Cd^{2+}$ after each experiment was recorded by atomic absorption spectrophotometer (Analytic Jena contra 300 Atomic Absorption, Germany). All instrumental measurements were achieved at the central laboratory of the Faculty of Science, Alexandria university.

### 2.3 Synthesis of ZnO NPs by plant extract

The leaves of *Ocimum tenuiflorum* plant (commonly known as Holy basil) were freshly collected, cleaned with running tap water to remove dirt, and then dried in sunlight. The dried powder was preserved in an airtight container. Ten grams of powdered leaves were added to 100 ml of deionized water then boiled for 10 min until the mixture turned red, then cooled. The leaf extract was centrifuged for 5 min at 5000 rpm, filtered, and refrigerated. ZnO NPs were produced by adding 2 ml of the *O. tenuiflorum* leaves aqueous extract dropwise to a 0.02 M solution of $Zn(CH_3COO)_2.2H_2O$ under conditions of continuous stirring in 70 °C water bath for 2 h. Drops of 0.5 M sodium hydroxide were added until pH ~ 12. The light-yellow precipitate of ZnO was formed. After repeated re-dispersions in deionized water, the precipitate was centrifuged and filtered. Calcination of the obtained precipitate was done in a ceramic crucible at 550 °C for 3 h [15, 26]. The yielded yellow powder was dried overnight at

80 °C and stored in airtight bottles for characterization. The preparation scheme is shown in Fig. S1.

## 2.4 Methodology

### 2.4.1 Batch equilibrium method

The adsorption capacity of the synthesized ZnO NPs for the metal ions under investigation ($Pb^{2+}$ and $Cd^{2+}$) was tested by the batch equilibrium method [17, 28]. A stock of adsorbate solution (1000 ppm) of each ion was prepared in deionized water. As an initial experimental condition, a certain amount of the green adsorbent was added and left in contact with the adsorbate solution under continuous stirring for 30 min in a rotary shaker at a rate of 150 rpm. Different experimental conditions including pH, adsorbent dosage, contact time, adsorbate concentration, and interfering ions were changed and tested separately to discover the optimum conditions of metal ions adsorption. After each experiment, the concentration of the residual metal ions in the filtrate was detected by AAS to evaluate the metal ions uptake.

### 2.4.2 Calculation of mass adsorption capacity

The mass adsorption capacity ($q_e$) and the percentage removal (% $R$) of the investigated metal ions ($Pb^{2+}$ and $Cd^{2+}$) by ZnO NPs were quantified by the following formulae [21]:

$$q_e = \frac{(C_o - C_e)V}{W}$$

$$\%R = \frac{(C_o - C_e) \times 100}{C_o}$$

where $C_o$ is the initial concentration of the metal ions in solution in ppm, $C_e$ is the concentration of the residual metal ions at equilibrium after applying the batch experiment, $V$ is the volume of solution in liter, and $W$ is the mass of ZnO NPs in grams.

### 2.4.3 Multistage microcolumn technique

The removal of heavy metals from real water samples by adsorption on the synthesized ZnO NPs was evaluated by the multistage microcolumn technique [26, 29]. The column was packed with 0.1 g of the sorbent. One liter of the water sample was pre-tested for the content of metal ions of interest and other physicochemical properties including percentage salinity ($S$%), pH, and oxidizable organic matter (OOM). Samples were also pre-tested for dissolved nutrient salts (nitrate ($NO_3$-N), nitrite ($NO_2$-N), dissolved inorganic phosphate (DIP), and dissolved inorganic silicate (DSi). Additionally, the major constituents $Ca^{2+}$, $Mg^{2+}$, $Na^+$, $Li^+$, $K^+$ were assessed, Table S1. Water samples were allowed to pass through the packed column at a slow flow rate of 0.5 ml $min^{-1}$. After the completion of three successive extractions, the filtrate was analyzed for $Cd^{2+}$ and $Pb^{2+}$ ions by AAS.

## 2.5 Cytotoxic screening against Panc-1, PC-3, CACO-2, and MRC-5

The cytotoxic activity of the green synthesized ZnO NPs was tested against three human cancer cell lines; pancreatic cancer cells (Panc-1), intestinal carcinoma cells (CACO-2), prostate cancer cells (PC-3), and normal human lung fibroblast cells (MRC-5) utilizing the colorimetric (MTT) assay, 3-(4,5-dimethylthiazole-2-yl)-2,5-diphenyltetrazolium bromide in a microtiter plate [30]. The results are indexed by $IC_{50}$ which represents the inhibition of the growth of the cells by 50% relative to cisplatin, the standard anticancer drug. The measurements were performed at the Regional Center for Mycology and Biotechnology, Al-Azhar University, Egypt. Of the seeded cells, 96-well plates were incubated at 37 °C for 24 h. Each sample concentration in DMSO was managed in triplicates and the results were averaged. All mammalian cell lines were obtained from the American Type Culture Collection (ATCC, Rockville, MD).

# 3 Results and discussion

## 3.1 Characterization of the synthesized ZnO NPs

### 3.1.1 FT-IR spectroscopy

FT-IR of the synthesized ZnO NPs exhibits six characteristic peaks (Fig. 1). The broad band at 3308 $cm^{-1}$ is assigned to the $\nu_{OH}$ of the phenolic group of the plant extract which is capping the particles. The small peak at 2344 $cm^{-1}$ is attributed to $\nu_{C\text{-}H}$. Also, the bands that appeared at 1493 and 1394 $cm^{-1}$ are due to the stretching vibrations of the C–N and –COO groups, respectively, which are the common functional groups of the *Ocimum tenuiflorum* plant that are accountable for the reduction of $Zn^{2+}$ ion and the formation of the metal nanoparticles [31]. Moreover, the band at 901 $cm^{-1}$ could be assigned to the bending mode of the O–H group. The sharp band that appeared at 474 $cm^{-1}$ is attributed to the metal–oxygen stretching which demonstrates the formation of ZnO NPs [32]. FT-IR spectra of the adsorbed $Pb^{2+}$ and $Cd^{2+}$ on ZnO NPs are shown in Fig. 1. Clear band shifts and intensity changes are observed in the FT-IR spectra after metal ion adsorption. For example, the disappearance of the bands at 3308 $cm^{-1}$ ($\nu_{O\text{–}H}$), 2344 $cm^{-1}$ ($\nu_{C\text{–}H}$) 1493 $cm^{-1}$ ($\nu_{C\text{–}N}$), and 1394 $cm^{-1}$ ($\nu_{COO}$) upon metal ions adsorption

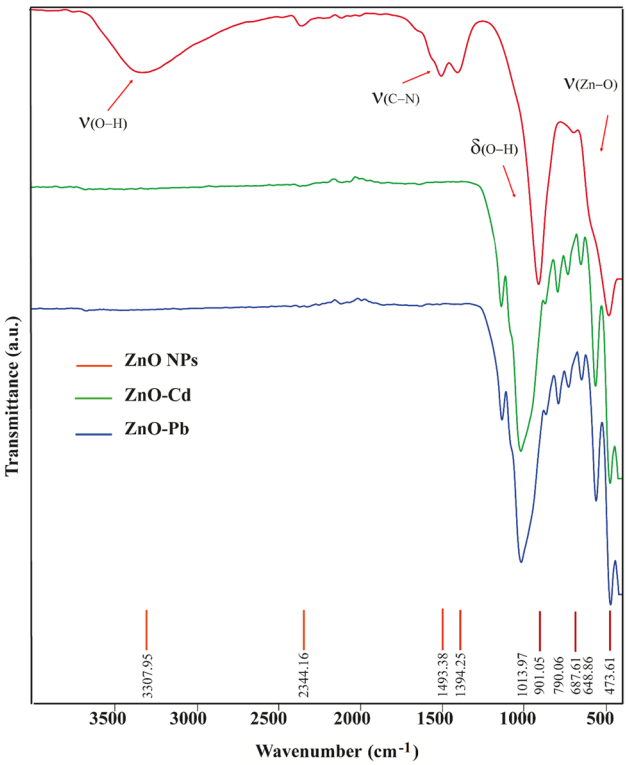


**Fig. 1** FT-IR of the synthesized free ZnO NPs (top) and the modified ZnO NPs after adsorption of $Cd^{2+}$ (middle) and $Pb.^{2+}$ (bottom)

indicates the role of these functional groups in the adsorption process. Besides, the emergence of new IR bands in the range 650–790 $cm^{-1}$ is assigned to the stretching vibration of Pb–O and Cd–O bonds [21, 33]. Also, the band at 901 $cm^{-1}$ ($\delta_{O-H}$) suffered a shift upon adsorption to 1014 and 1016 $cm^{-1}$ for $Cd^{2+}$ and $Pb^{2+}$, respectively, which is further evidence of the involvement of the O–H group in the adsorption process.

### 3.1.2 X-ray diffractometry (XRD)

Eight Sharp XRD peaks of the synthesized ZnO NPs were recorded (Fig. 2). The values of lattice spacing (*d*) corresponding to each diffraction angle with their intensity counts are displayed in Table S2. The peaks located at Bragg's diffraction angles (2*θ*) of 31.73°, 34.38°, 36.23°, 47.50°, 56.59°, 62.77°, 67.96°, and 69.12° were assigned to the planes (100), (002), (101), (102), (110), (103), (112), and (201) according to the Joint Committee of Powder Diffraction Standards of ZnO file (JCPDS 36–1451) [34]. The diffraction results confirmed the crystallization of the synthesized ZnO NPs in the hexagonal wurtzite structure which is the most stable and common form at normal conditions of temperature and pressure [35]. Also, the experimental interplanar spacing 2.817 Å, 2.60 Å, and 2.477 Å were in excellent agreement with the standard values of JCPDS 2.814 Å (100), 2.603 Å (002), and 2.476 Å (101) for hexagonal ZnO.

### 3.1.3 Scanning electron microscopy (SEM), transmission electron microscope (TEM), and energy-dispersive X-ray (EDX)

The surface morphology of the synthesized ZnO NPs was examined by SEM technique. The images (Fig. 3) show that the particles have spherical shapes of particle sizes ~ 19 nm. No evidence of aggregation was observed in the scan which is due to the stabilization of nanoparticles by the plant extract. SEM images of the surface of ZnO nanosphere after the adsorption of $Cd^{2+}$ and $Pb^{2+}$ (Fig. 4) demonstrate clear changes owing to the occupation of the active sites by these metal ions yielding a non-uniform covering around the ZnO NPs surface. The observed changes on the surface verified the physical adsorption mechanism [36]. The particle size of the

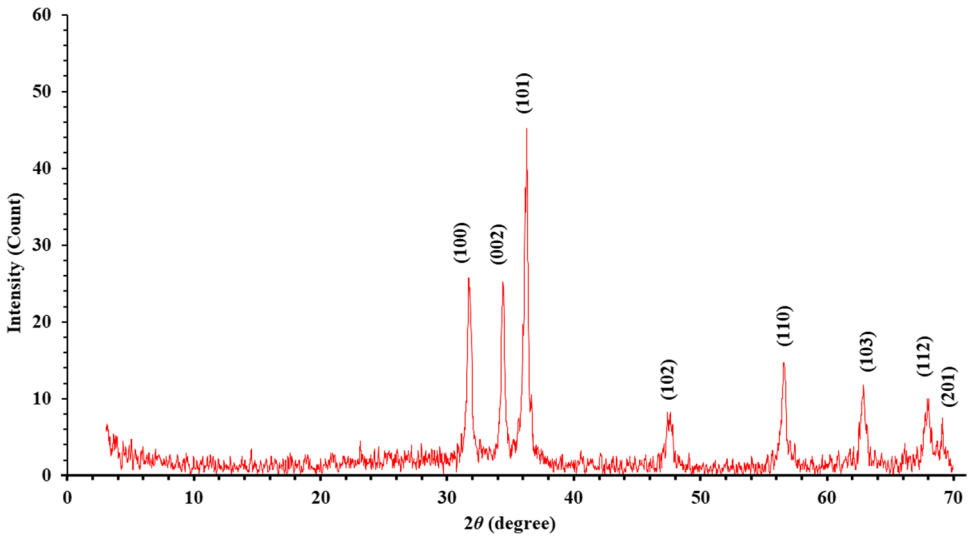


**Fig. 2** XRD pattern of the synthesized ZnO NPs using Cu anode at $\lambda = 1.5406$ Å

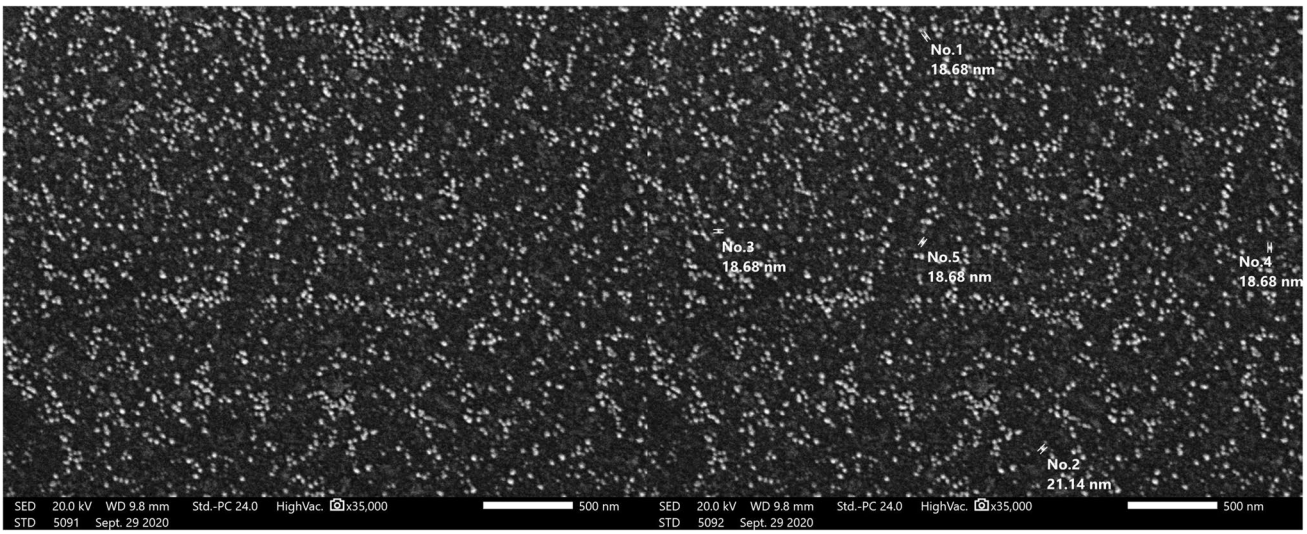


**Fig. 3** SEM of ZnO NPs showing the spherical nature of the particles with a size of 18.68 nm

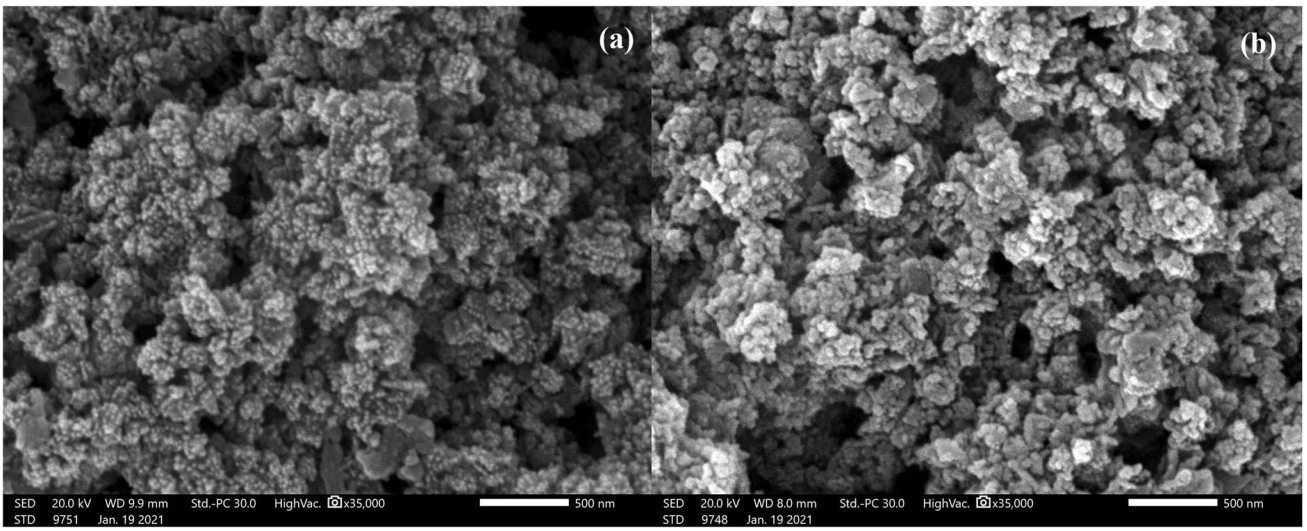


**Fig. 4** Morphology changes due to the adsorption of (**a**) $Cd^{2+}$ and (**b**) $Pb^{2+}$ on ZnO NPs

synthesized ZnO NPs was further approved by the TEM technique (Fig. 5). Also, the connection of EDX to the SEM technique provides a tool to identify the elemental composition of the scanned sample. EDX spectrum (Fig. 6) revealed that the abundant elements in the synthesized ZnO NPs are zinc and oxygen at binding energies of 1 and 0.5 keV with measured mass percent of 56.17 and 39.08%, respectively [37]. No discernible peak was noted for impurities. The data point to the high purity of the synthesized ZnO nanoparticles [34].

### 3.2 Effect of pH, adsorbent dosage, contact time, initial metal ion, and interfering ions concentrations on the adsorption capacity

The adsorption of $Pb^{2+}$ and $Cd^{2+}$ by the synthesized ZnO NPs was measured at pH range (2–7) at room temperature by the batch equilibrium approach where 0.02 g of ZnO was added to 25 ml of samples loaded with equimolar of the tested ions. The maximum adsorption of $Pb^{2+}$ and $Cd^{2+}$ (96.73% and 21.35%, respectively) was achieved at pH = 7

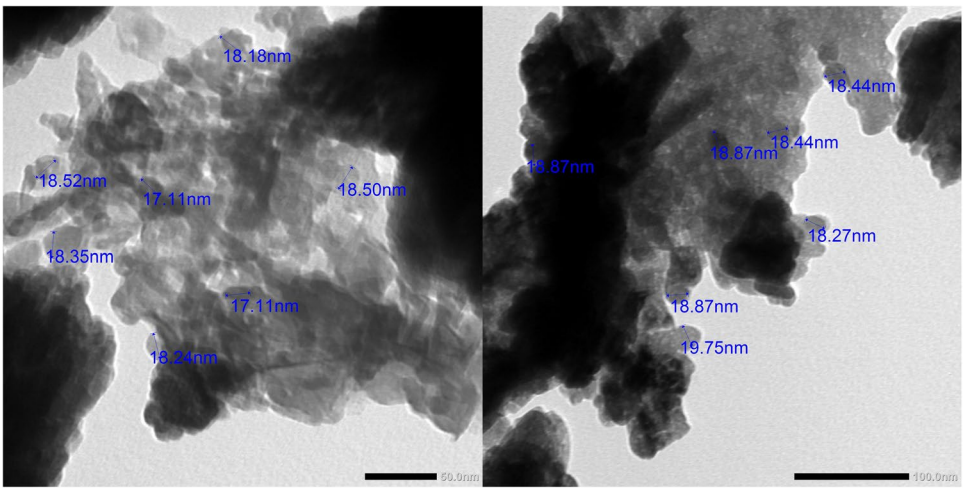


**Fig. 5** Images of the synthesized ZnO NPs by TEM technique

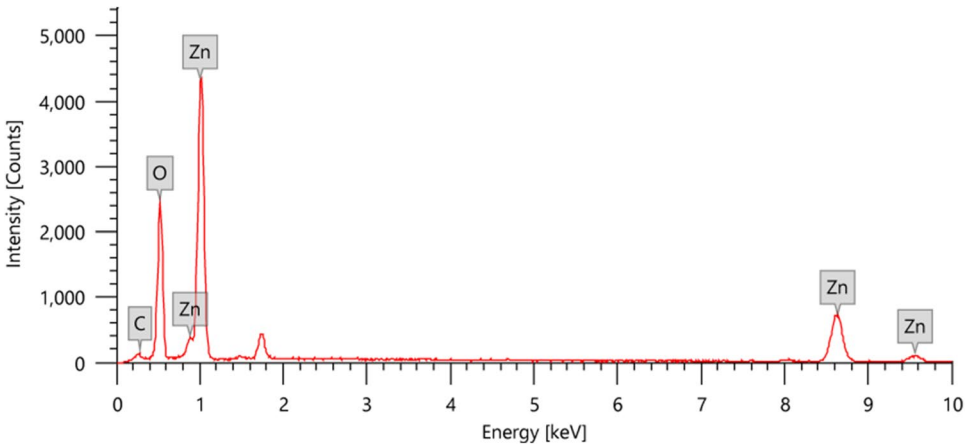


**Fig. 6** EDX profile of the synthesized ZnO NPs

**Table 1** The impact of pH on the % removal and metal sorption capacity ($mgg^{-1}$) of ZnO NPs

| pH | | 2 | 3 | 4 | 5 | 6 | 7 |
|---|---|---|---|---|---|---|---|
| $Pb^{2+}$ | $q_e$ | 0.02 | 0.66 | 0.98 | 6.20 | 20.27 | 24.18 |
| | % Removal | 0.10 | 2.65 | 3.90 | 24.80 | 81.08 | 96.73 |
| $Cd^{2+}$ | $q_e$ | 0.45 | 0.99 | 1.48 | 1.95 | 3.61 | 5.34 |
| | % Removal | 1.80 | 3.95 | 5.90 | 7.80 | 14.45 | 21.35 |

(Table 1). Generally, the small size and the high mobility of hydrogen ions in solutions result in a higher affinity for adsorption on surfaces than the affinity for $Pb^{2+}$ and $Cd^{2+}$ [38, 39]. Therefore, the high concentration of hydrogen ions at low pH values leads to great competition between protons and metal ions for the active sorption sites, and hence low adsorption capacity was observed for the investigated metal ions in the strong acidic solutions. However, at pH > 5, the deprotonation of the surface enhances the uptake of the metal ions from the surrounding medium. Also, the adsorption capacity ($q_e$) values detected at pH 7 for $Cd^{2+}$ and $Pb^{2+}$ are 24.18 and 5.34 $mgg^{-1}$, respectively. This implies high selectivity of ZnO NPs material for $Pb^{2+}$ compared to $Cd^{2+}$.

Additionally, the impact of sorbent dosage on the $Pb^{2+}$ and $Cd^{2+}$ removing capacity was determined at various weights in the range of 10–200 mg of ZnO NPs at the optimum pH value (pH = 7). The results showed that the maximum adsorption capacity for $Pb^{2+}$ ($q_e = 25$ $mgg^{-1}$) was achieved at a sorbent dosage of 40 mg of ZnO NPs. However, the adsorption of $Cd^{2+}$ exhibited high value ($q_e = 25$ $mgg^{-1}$) at 200 mg of ZnO NPs (Fig. 7). Noteworthy, the small sorbent dosage required for the maximum removal of ions is good evidence for the efficiency of ZnO NPs as an adsorbing surface.

Also, the optimal contact time for the adsorption of $Pb^{2+}$ and $Cd^{2+}$ on the surface of ZnO NPs was assessed at time intervals between 10 and 60 min and under the optimum

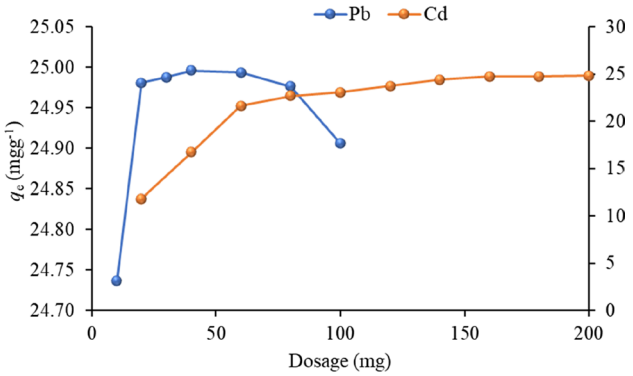


**Fig. 7** The adsorption capacity of $Pb^{2+}$ and $Cd^{2+}$ at different dosages of ZnO NPs

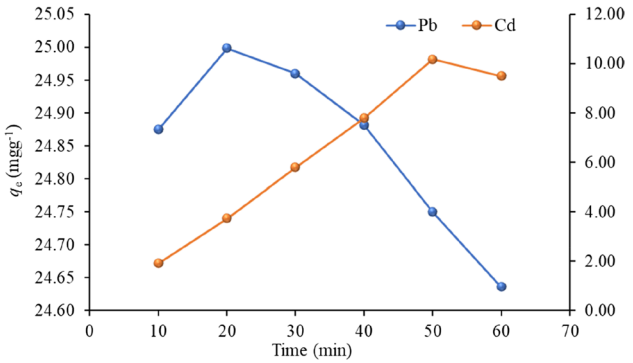


**Fig. 8** The time-dependent adsorption of $Pb^{2+}$ and $Cd^{2+}$ by ZnO NPs

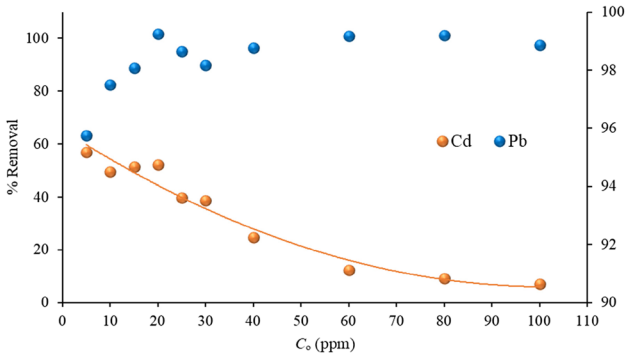


**Fig. 9** The effect of initial concentration of $Pb^{2+}$ and $Cd^{2+}$ on their % removal by ZnO NPs

**Table 2** The effect of interfering ions on the percentage removal and metal sorption capacity (mgg$^{-1}$) of $Cd^{2+}$ and $Pb^{2+}$ on ZnO NPs

| Interfering ions | $Cd^{2+}$ | | $Pb^{2+}$ | |
|---|---|---|---|---|
| | % Removal | $q_e$ (mgg$^{-1}$) | % Removal | $q_e$ (mgg$^{-1}$) |
| Blank | 98.32 | 0.62 | 99.61 | 12.45 |
| NaCl | 73.48 | 0.46 | 94.46 | 11.81 |
| KCl | 85.06 | 0.53 | 93.85 | 11.73 |
| $MgSO_4$ | 85.45 | 0.53 | 93.56 | 11.70 |
| $KNO_3$ | 95.04 | 0.59 | 93.79 | 11.72 |
| $Na_2CO_3$ | 97.00 | 0.61 | 89.90 | 11.24 |
| $CaCO_3$ | 97.22 | 0.61 | 94.24 | 11.78 |

experimental conditions for each investigated ion. Clearly, the mechanism started with rapid adsorption of the positive ions on the surface of ZnO NPs (Fig. 8) which was then slowed after the saturation of most of the available active sites. The maximum adsorption of $Cd^{2+}$ was obtained at 50 min with removal percentage and capacity of metal sorption are 40.7% and 10.18 mgg$^{-1}$, respectively. On the other hand, the adsorption of $Pb^{2+}$ reached its maximum at a contact time of 20 min with removal percentage and capacity of metal sorption values of 99.99% and 25 mgg$^{-1}$, respectively. In the current work, the detected short equilibrium contact time for the adsorption of $Pb^{2+}$ provides an economic benefit for large-scale wastewater treatment applications.

Moreover, the effect of the initial metal ion concentration ($C_\circ$) on the adsorption capacity was tested at different $Pb^{2+}$ and $Cd^{2+}$ concentration values in the range of 5–100 ppm at the optimum pH, sorbent dose, and contact time. The profile of percentage metal ions removal as a function of initial metal ions concentration (Fig. 9) revealed a primarily increase in the metal uptake with the increase of $Pb^{2+}$ concentration. However, at higher concentrations of the tested ion, the removal decreases probably due to the surface saturation. Maximum removal of 99.24% of $Pb^{2+}$ from the solution was attained by using an initial concentration of ($C_\circ = 20$ ppm). However, the peak adsorption for $Cd^{2+}$ corresponds to a removal of 56.98% was reached early at $C_\circ = 5$ ppm (Fig. 9). This was followed by a rapid decline in adsorption due to fewer available sites for adsorption. The results imply that ZnO NPs have a high adsorption affinity for $Pb^{2+}$, and hence is an efficient adsorbent for the elimination of this ion from aqueous solutions [40]. The data of the adsorption experiments were fitted to different isotherm and kinetic models.

Based on the batch experiments, the optimum adsorption conditions for the two investigated ions were established. The initial concentration of 5 ppm $Cd^{2+}$, contact time = 50 min., and 200 mg ZnO NPs were the best conditions in the case of $Cd^{2+}$. However, 20 ppm $Pb^{2+}$, contact time = 20 min, and 40 mg ZnO NPs are the condition for maximum adsorption of $Pb^{2+}$. Furthermore, the influence of interfering ions, on the adsorption capacity of ZnO NPs was examined by adding 25 ml of 0.1 g of some selected ions, NaCl, KCl, $MgSO_4$, $KNO_3$, $NaCO_3$, and $CaCO_3$ in deionized water to the standard solution containing $Cd^{2+}$ and $Pb^{2+}$ under the optimum experimental adsorption conditions at pH = 7. The results are summarized in Table 2. Generally, ions that coexist in solutions greatly hinder the adsorption

of the ions of interest by competing for the sorbents' active sites. The mechanism is mainly governed by the hydrated radius which is inversely related to the ionic radius and to the affinity of adsorption [41]. The small hydration shell of $Pb^{2+}$ facilitates its mobility across the boundary layer of the adsorbent surface [42]. In the present work (Table 2), the absence of interfering ions yields the highest adsorption capacity towards $Cd^{2+}$ and $Pb^{2+}$ with a percentage removal of 98.32 and 99.61%, respectively. The results showed that NaCl ions exhibited the highest interfering effect in the case of the $Cd^{2+}$ adsorption which lowered the removal percentage of $Cd^{2+}$ by about 25%. However, $Na_2CO_3$ and $CaCO_3$ cause insignificant changes in the adsorption capacity of $Cd^{2+}$. Besides, most of the selected ions did not interfere significantly in the removal of $Pb^{2+}$ by ZnO NPs except for the $Na_2CO_3$ which causes a reduction in the efficiency of $Pb^{2+}$ removal by about 10%.

## 3.3 Adsorption modeling

### 3.3.1 Isotherm models

Four different isotherm models, namely Langmuir, Freundlich, Tempkin, and Dubinin–Radushkevich, were fitted to the adsorption data of $Cd^{2+}$ and $Pb^{2+}$ ions on ZnO NPs to correlate the experimental results with the model. The best-fitting model displayed a correlation coefficient ($R^2$) equal to unity [43]. The model equations with the definition of each parameter are stated in the supplementary data, Table S3. Also, the calculated parameters of the isotherm models are collected in Table 3. Langmuir isotherm assumes that adsorption is a monolayer formation process where one ion is adsorbed per active site with all spots being energetically equivalent, and no interaction occurs between the adsorbed ions [44]. The results revealed that the experimental data for the adsorption of $Cd^{2+}$ and $Pb^{2+}$ on ZnO NPs fitted well to the Langmuir isotherm (Fig. 10), with a correlation coefficient of $R^2 = 0.9659$ and 0.8557, respectively. Also, the maximum adsorption capacity ($q_{max}$) of the adsorption of $Pb^{2+}$ is almost twice the adsorption of $Cd^{2+}$. Moreover, the separation factor $R_L$ (Table S3) indexes the feasible nature of adsorption in the Langmuir isotherm. Under the current experimental conditions, the calculated low value of $R_L$ (0.01–0.69) indicates that the adsorption is favorable [45].

Likewise, the experimental data demonstrated a good fit to Freundlich isotherm (Fig. 11 and Tables S3 & 3), with $R^2 = 0.9600$ and 0.9295 for $Pb^{2+}$ and $Cd^{2+}$, respectively. This isotherm states that the concentration of ions adsorbed on the sorbent surface increases with the concentration of the adsorbate with the possibility of multi-layers formation. The

**Table 3** Calculated isotherm model parameters for the adsorption of $Pb^{2+}$ and $Cd^{2+}$ ions on ZnO NPs

| Equilibrium models | Parameters | $Pb^{2+}$ | $Cd^{2+}$ |
|---|---|---|---|
| Langmuir | $q_{max}$ experimental | 123.57 | 14.45 |
| | $q_{max}$ ($mgg^{-1}$) | 44.84 | 22.03 |
| | $K_L$ ($Lmg^{-1}$) | 0.98 | 0.09 |
| | $R^2$ | 0.856 | 0.966 |
| Freundlich | $K_f$ ($Lmg^{-1}$) | 12.67 | 1.43 |
| | $n_f$ ($gL^{-1}$) | 0.41 | 1.498 |
| | $1/n_f$ ($Lg^{-1}$) | 2.46 | 0.67 |
| | $R^2$ | 0.960 | 0.929 |
| Tempkin | $A_t$ ($Lmg^{-1}$) | 4.55 | 0.860 |
| | $B_T$ ($kJmol^{-1}$) | 89.79 | 5.22 |
| | $R^2$ | 0.972 | 0.918 |
| Dubinin–Radushkevich (D-R) | $q_m$ ($mgg^{-1}$) | 209.9 | 13.09 |
| | $K_{DR}$ | $2\times10^{-7}$ | $1\times10^{-6}$ |
| | $R^2$ | 0.931 | 0.963 |
| | $E_D$ ($kJmol^{-1}$) | 1.581 | 0.707 |

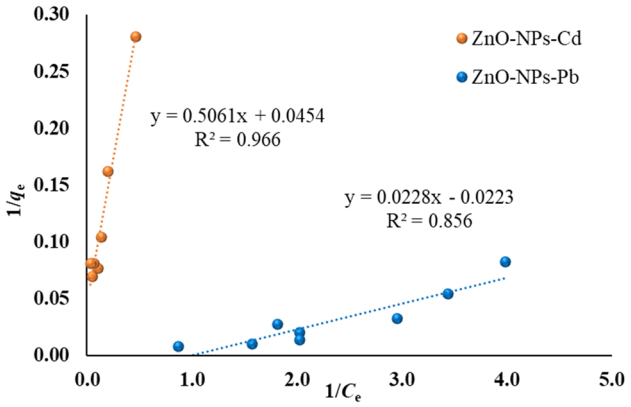


**Fig. 10** Langmuir adsorption isotherm for the adsorption of $Cd^{+2}$ and $Pb^{+2}$ by ZnO NPs

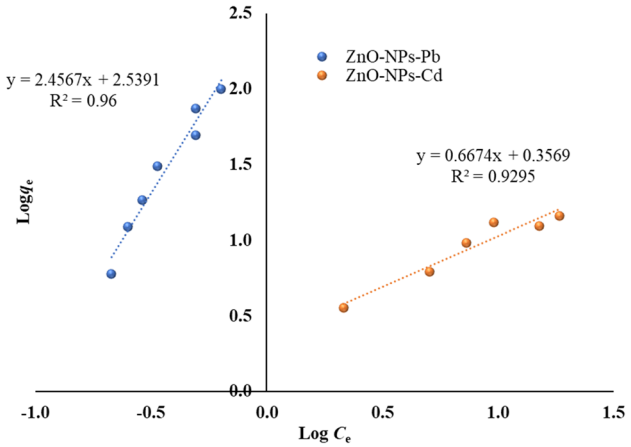


**Fig. 11** Freundlich adsorption isotherm for the adsorption of $Cd^{+2}$ and $Pb^{+2}$ by ZnO NPs

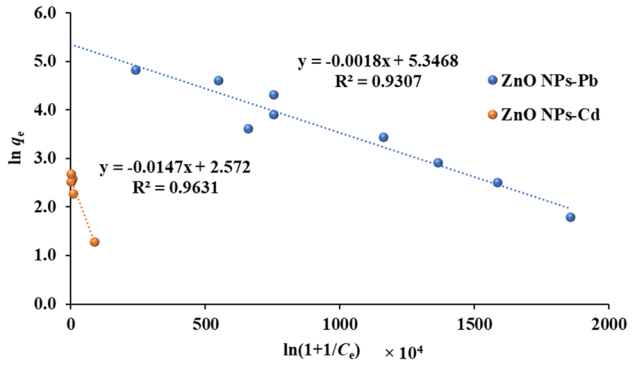


**Fig. 12** D-R model for the adsorption of $Cd^{2+}$ and $Pb^{2+}$ by ZnO NPs at room temperature

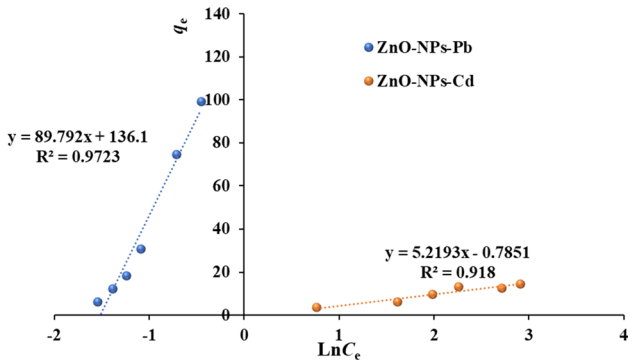


**Fig. 13** Tempkin model for the adsorption of $Cd^{2+}$ and $Pb^{2+}$ by ZnO NPs at room temperature

value of the adsorption intensity ($n$) being greater than one in the case of the $Cd^{2+}$ adsorption indicates the ease of ions separation from solution and hence the viability of adsorption [46].

Furthermore, the physical or chemical nature of the adsorption process can be justified by Dubinin–Radushkevich's isotherm (D-R) isotherm (Table S3 and 3). Physical adsorption is assigned for systems with apparent energy also called the mean free energy, $E_D$, in the range (1–8) $kJmol^{-1}$ [47]. Based on the calculated D-R parameters, the experimental data fitted well with the (D-R) isotherm model, $R^2 = 0.931$ and 0.963 for $Pb^{2+}$ and $Cd^{2+}$, respectively (Fig. 12). The calculated $E_D$ values for the current work, 1.58 and 0.707 $kJmol^{-1}$ confirm that the adsorption is a physisorption process [48]. Tempkin isotherm (Table S3 & 3) is a useful model to predict the heat of adsorption. The graphs of $q_e$ versus ln $C_e$ (Fig. 13) showed a linear relation with a correlation coefficient of 0.972 and 0.918 for $Pb^{2+}$ and $Cd^{2+}$, respectively, indicating the viability of Tempkin's isotherm. The Tempkin parameters, variation of the heat of adsorption ($B_T$) and the equilibrium binding constant ($A_T$), can be extracted from the slope and the intercept of the linear plot, respectively. The positive value of $B_T$ point to an exothermic adsorption process. Also, the affinity of $Pb^{2+}$ to the active sites at ZnO NPs is greater ($A_T = 4.55$ $Lmg^{-1}$) than the affinity toward $Cd^{2+}$ ($A_T = 0.68$ $Lmg^{-1}$) which suggests an extent of selectivity of the surface to $Pb^{2+}$ [49]. Furthermore, the heat of adsorption ($B_T$) are found to be 0.027 and 0.474 $KJmol^{-1}$ for $Pb^{2+}$ and $Cd^{2+}$ at $T = 298$ K.

### 3.3.2 Kinetics of adsorption

Four kinetic models were employed to assess the mechanism of adsorption process of metal ions on the synthesized ZnO NPs. The results of the batch adsorption experiments were fitted to pseudo-first-order, second-order, liquid film, and intraparticle diffusion kinetic models (Table S4). The fitting results revealed a good agreement with the second-order model where the calculated correlation coefficient values are of about unity (Table 4). Also, applying the second-order model yielded a calculated adsorption capacity $q_e$, which is in accord with the experimental values (Table 4),

**Table 4** Fitting parameters of pseudo-first-order and second-order kinetic models for the $Cd^{2+}$ and $Pb^{2+}$ adsorption by ZnO NPs

| Metal ions | $C_\circ$ (ppm) | $q_e$ (exp.) ($mgg^{-1}$) | Pseudo-first-order kinetics | | | Pseudo-second-order kinetics | | |
|---|---|---|---|---|---|---|---|---|
| | | | $k_1$ | $q_e$ (calc.) | $R^2$ | $k_2$ | $q_e$ (calc.) | $R^2$ |
| $Pb^{2+}$ | 5 | 3.05 | 0.054 | 6.07 | 0.865 | 1.38 | 3.04 | 0.9999 |
| | 10 | 6.02 | 0.050 | 4.044 | 0.761 | 0.56 | 6.03 | 0.9999 |
| | 15 | 8.89 | 0.040 | 1.49 | 0.675 | 0.17 | 8.91 | 0.9996 |
| | 20 | 12.25 | 0.013 | 3.00 | 0.328 | 3.12 | 12.06 | 0.9999 |
| | 25 | 15.09 | 0.031 | 7.22 | 0.360 | 0.73 | 15.08 | 1.000 |
| | 30 | 18.33 | 0.053 | 4.14 | 0.519 | 0.38 | 18.38 | 1.000 |
| $Cd^{2+}$ | 5 | 0.48 | 0.056 | 7.90 | 0.856 | 0.74 | 0.50 | 0.9985 |
| | 10 | 0.93 | 0.042 | 4.38 | 0.732 | 1.01 | 0.76 | 0.9807 |
| | 15 | 1.85 | 0.053 | 2.47 | 0.546 | 0.53 | 1.87 | 0.9893 |
| | 20 | 2.48 | 0.026 | 4.04 | 0.566 | 0.61 | 1.99 | 0.9742 |
| | 25 | 3.09 | 0.098 | 1.95 | 0.875 | 0.33 | 3.02 | 0.9966 |
| | 30 | 3.73 | 0.049 | 2.54 | 0.711 | 0.40 | 3.10 | 0.9709 |

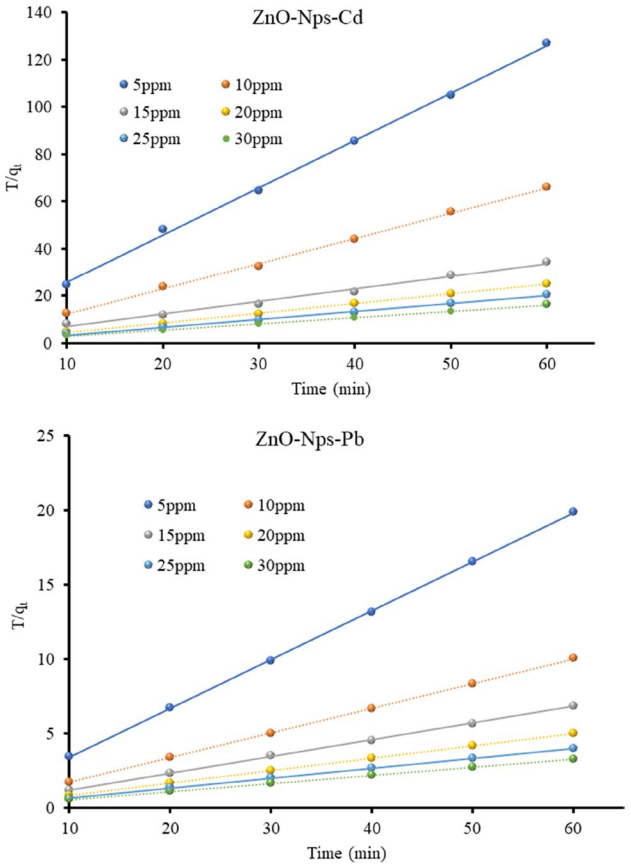


**Fig. 14** Pseudo-second-order kinetic plots of metal ions adsorption by ZnO NPs

with a perfect linear relation along the whole range of the metal ion concentration (Fig. 14). The excellent fitting of the experimental data to the second-order model implies kinetic mechanism that involves both the metal ion and the surface where the rate-determining step is electron exchange between these two entities [50]. Moreover, to evaluate the nature of the diffusion process that took place in the bulk system prior to the adsorption, intraparticle diffusion and liquid film diffusion models were applied (Table S4). Noticeably, there is a clear divergence from linearity between the experimental results and the intraparticle diffusion model with a low calculated correlation coefficient $R^2$ being in the range 0.196–0.845 (Table S5). This divergence from the model ruled out the dominance of intraparticle diffusion in controlling the adsorption mechanism. However, fitting the data to the liquid film diffusion model (Table S4) showed better correlation values ($R^2$ is in the range 0.6783–0.9897, Table S5) which suggests that the mechanism is mainly governed by the liquid film surrounding the adsorbent surface. Nevertheless, the deviation of the straight lines of the film model from passing through the origin (Fig. S2) indicates the existence of a combination of different diffusion mechanisms leading to a heterogeneous diffusion process [51].

### 3.4 *Adsorption of $Cd^{2+}$ and $Pb^{2+}$ from environmental water samples*

The applicability of the green synthesized ZnO NPs for the elimination of $Cd^{2+}$ and $Pb^{2+}$ from environmental water samples was investigated by using a multistage column packed with the sorbent. Samples were gathered from distinct locations to represent different types of water. For example, El-Mex Bay sample represents the polluted brackish water and the sample collected from the West Dessert Operating Petroleum Company discharge exemplifies the wastewater. Samples were also taken from the Eastern Harbor to represent normal seawater and El-Mahmoudia Canal as freshwater. The characteristic physicochemical parameters of each sample are measured and listed in Table S1. The removal percentages in each run of the adsorption of $Cd^{2+}$ and $Pb^{2+}$ from the samples are shown in Table 5. Undoubtedly, the best metal ions removal was extracted after the third run of the experiment, where the percentage removal reached 99.95% in the case of the Petroleum Company sample. After the three consecutive extractions, the % removal of $Cd^{2+}$ and $Pb^{2+}$ were in the range 48.82–97.36% and 94.93–99.95%, respectively, which points to the feasibility of adsorption of $Pb^{2+}$ compared to $Cd^{2+}$. This detected selectivity of ZnO NPs towards $Pb^{2+}$ has been previously reported [26] and it could be explained by the difference in ionic radius, hydration diameters, and solubility between these ions. Also, the high percentage elimination of $Cd^{2+}$ from the Freshwater (El-Mahmoudia Canal, 97.36%) implies that interfering ions in these samples have a big influence on adsorption. Moreover, the less removal percentage of the heavy metals of interest from El-Mex Bay station may be due to different impurities and high concentrations of

**Table 5** Percentage removal of $Cd^{2+}$ and $Pb^{2+}$ by the green sorbent ZnO NPs from environmental samples

| Investigated metal ions | $Cd^{2+}$ (%Removal) | | | $Pb^{2+}$ (%Removal) | | |
|---|---|---|---|---|---|---|
| Water sample | Run1 | Run2 | Run3 | Run1 | Run2 | Run3 |
| Petroleum Co | 80.77 | 82.23 | 83.53 | 82.24 | 84.26 | 99.95 |
| El-Mahmoudia Canal | 87.18 | 91.67 | 97.36 | 85.61 | 94.44 | 97.97 |
| El-Mex Bay | 33.85 | 39.11 | 48.82 | 91.12 | 94.73 | 94.93 |
| Eastern Harbor | 36.07 | 41.49 | 49.89 | 96.94 | 97.06 | 99.37 |

nutrient salts (Table S1). The outlined results in this contribution provide evidence that ZnO NPs synthesized by plant extract are efficient low-cost surface for the removal of $Cd^{2+}$ and $Pb^{2+}$ from water samples.

### 3.5 Cytotoxic activity of the green synthesized ZnO NPs

The antiproliferative activity of the green synthesized ZnO NPs has been examined against three mammalian cancer cell lines: Panc-1 (human pancreatic cancer cell line), PC-3 (human prostate carcinoma), and CACO-2 (intestinal carcinoma) as presented in Table 6. The cytotoxicity of ZnO NPs was also investigated versus normal human lung cell MRC-5. The concentrations of ZnO NPs required to inhibit 50% of the examined cells, $IC_{50}$, are extracted from the graphical relation between the applied ZnO NPs concentrations and the surviving cells (Fig. 15(a–c)), where the viable cells were identified by a colorimetric technique using the MTT method. Many reports have proposed mechanisms of ZnO NPs cytotoxicity against cancers. ZnO NPs is approved to induce oxidative stress inside the cancer cell by increasing the level of reactive oxygen which leads to cell death after the formation of lipid peroxides and the damage of cell protein [52, 53]. Also, the nanoparticles cause a series of observed cell alterations including cell rounding and shrinkage, chromatin aggregation, and the formation of apoptotic bodies that leads to cell apoptosis [12, 54, 55]. In the present study, a superior activity for ZnO NPs against the tested cancer cells has been observed. The high inhibitory activities of the synthesized ZnO NPs (1.70, 3.67, and 5.70 $\mu gml^{-1}$) compared to that of the standard therapeutic agent, cisplatin, (3.57, 5.09, 7.75 $\mu gml^{-1}$) under the same experimental conditions, points to a promising anticancer candidate. Moreover, the low inhibition efficacy of ZnO NPs against normal cells, MRC-5, implies its potency as a selective low side effect anticancer drug. Furthermore, comparison of the cytotoxic activity of the synthesized ZnO NPs with cisplatin revealed that they exerted nearly equipotency against the normal cell MRC-5 with IC50 of $22.40 \pm 1.28$ and $22.50 \pm 0.73$ respectively (Fig. 16).

**Table 6** Cytotoxicity activity ($IC_{50}$) in $\mu gml^{-1}$ of the green synthesized ZnO NPs

| Compounds | Tumor cell lines | | | Normal cell line MRC-5 |
|---|---|---|---|---|
| | Panc-1 | PC-3 | CACO-2 | |
| ZnO NPs | $1.70 \pm 0.23$ | $3.67 \pm 0.41$ | $5.70 \pm 0.68$ | $22.40 \pm 1.28$ |
| Cisplatin | $3.57 \pm 0.29$ | $5.09 \pm 0.31$ | $7.75 \pm 0.89$ | $22.50 \pm 0.73$ |

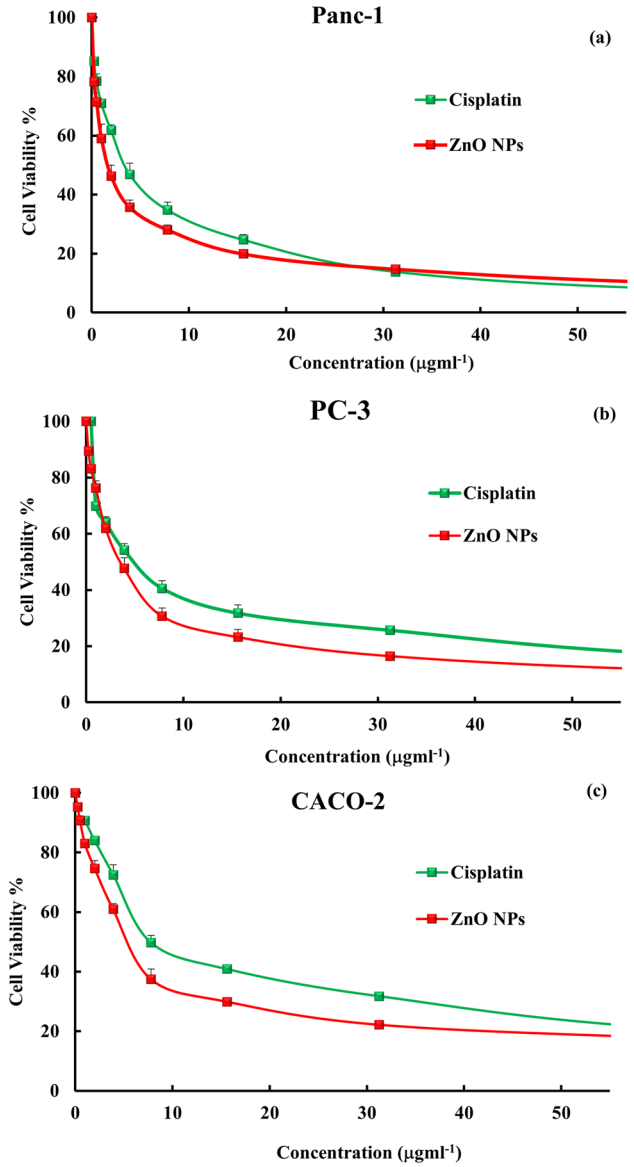


**Fig. 15** Antiproliferative activity of ZnO NPs against (**a**) Panc-1, (**b**) PC-3, and (**c**) CACO-2

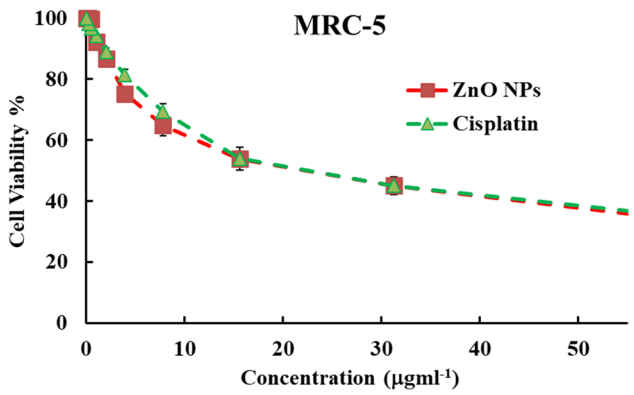


**Fig. 16** Cytotoxic activity of ZnO NPs and cisplatin against normal human lung cells

## 4 Conclusion

Nano-ZnO was synthesized by an eco-friendly method and then carefully characterized by different spectroscopic techniques. The synthesized ZnO NPs showed significant adsorption capacity for $Pb^{2+}$ and $Cd^{2+}$ at pH = 7. The short contact time required for the maximum adsorption of $Pb^{2+}$ (20 min) pointed to a high degree of selectivity of ZnO to this ion. Perfect removal of $Cd^{2+}$ and $Pb^{2+}$ from environmental water samples was accomplished where the highest removal percentage was observed at El -Mahmoudia Canal with a percentage removal of 97.36% and 97.97% for $Cd^{2+}$ and $Pb^{2+}$ respectively. The synthesized green sorbent showed substantial efficiency in the metal ions elimination, and hence can be considered a promising eco-friendly and low-cost agent in the remediation of polluted water. Cytotoxic activity of ZnO NPs is another important application that was explored in the current work. The three investigated cancer cell lines (Panc-1, PC-3, and CACO-2) were extremely sensitive to ZnO NPs with $IC_{50}$ of 1.70, 3.67 and 5.70 $\mu g ml^{-1}$ respectively. The detected activity was more potent than that of cisplatin, the standard anticancer drug. Interestingly, the nanoparticles exhibited less inhibition effect on the normal cell (MRC-5) compared to their effect on cancer cells. The cytotoxic results shed light on the ZnO NPs synthesized using *Ocimum tenuiflorum* leaves as promising highly effective, low-price, and low-side effects antiproliferative agent. The combination of reaction conditions, precursors, as well as the method of preparation used in the present contribution, is considered a novel practice that yielded ZnO nanoparticles of very small size (18.68 nm) which led to high removal capacity of $Pb^{2+}$ and $Cd^{2+}$ and superior cytotoxicity against the investigated cancer cell lines.

**Supplementary Information** The online version contains supplementary material available at https://doi.org/10.1007/s13399-022-03709-1.

**Acknowledgements** The authors are grateful to Alexandria University, Egypt for supporting this investigation.

**Author contribution** Idea and protocol design: Rehab M. I. Elsamra, Mamdouh S. Masoud, Mohamed A. Okbah, Alyaa A. Zidan, Gehan M. El Zokm. Methodology and experimentation: Alyaa A. Zidan, Rehab M. I. Elsamra, Gehan M. El Zokm. Data analysis: Rehab M. I. Elsamra, Gehan M. El Zokm, Alyaa A. Zidan. All authors shared draft writing. All authors approved the submission.

**Funding** Open access funding provided by The Science, Technology & Innovation Funding Authority (STDF) in cooperation with The Egyptian Knowledge Bank (EKB).

**Data availability** The data that support the findings of this study are available in the supplementary material.

## Declarations

**Competing interests** The authors declare no competing interests.

**Open Access** This article is licensed under a Creative Commons Attribution 4.0 International License, which permits use, sharing, adaptation, distribution and reproduction in any medium or format, as long as you give appropriate credit to the original author(s) and the source, provide a link to the Creative Commons licence, and indicate if changes were made. The images or other third party material in this article are included in the article's Creative Commons licence, unless indicated otherwise in a credit line to the material. If material is not included in the article's Creative Commons licence and your intended use is not permitted by statutory regulation or exceeds the permitted use, you will need to obtain permission directly from the copyright holder. To view a copy of this licence, visit http://creativecommons.org/licenses/by/4.0/.

## References

1. Srujana S, Bhagat D (2022) Chemical-based synthesis of ZnO nanoparticles and their applications in agriculture. Nanotechnol Environ Eng 7(1):269–275. https://doi.org/10.1007/s41204-022-00224-6
2. Fouda A, Saad EL, Salem SS, Shaheen TI (2018) In-vitro cytotoxicity, antibacterial, and UV protection properties of the biosynthesized zinc oxide nanoparticles for medical textile applications. Microb Pathog 125:252–261. https://doi.org/10.1016/j.micpath.2018.09.030
3. Saravanan P, SenthilKannan K, Divya R, Vimalan M, Tamilselvan S, Sankar D (2020) A perspective approach towards appreciable size and cost-effective solar cell fabrication by synthesizing ZnO nanoparticles from *Azadirachta indica* leaves extract using domestic microwave oven. J Mater Sci Mater Electron 31(5):4301–4309. https://doi.org/10.1007/s10854-020-02985-9
4. Kumar V, Gohain M, Som S, Kumar V, Bezuindenhoudt BC, Swart HC (2016) Microwave assisted synthesis of ZnO nanoparticles for lighting and dye removal application. Phys B Condens Matter 480:36–41. https://doi.org/10.1016/j.physb.2015.07.020
5. Yu W, Zhang J, Peng T (2016) New insight into the enhanced photocatalytic activity of N-, C-and S-doped ZnO photocatalysts. Appl Catal B Environ 181:220–227. https://doi.org/10.1016/j.apcatb.2015.07.031
6. Mohamed YMA, Attia YA (2020) The influence of ultrasonic irradiation on catalytic performance of ZnO nanoparticles toward the synthesis of chiral 1-substituted-1H-tetrazolederivatives from α-amino acid ethyl esters. Appl Organomet Chem 34(9):e5758. https://doi.org/10.1002/aoc.5758
7. Dhiman V, Kondal N (2021) ZnO Nanoadsorbents: a potent material for removal of heavy metal ions from wastewater. Colloid Interface Sci Commun 41:100380. https://doi.org/10.1016/j.colcom.2021.100380
8. Ghule K, Ghule AV, Chen BJ, Ling YC (2006) Preparation and characterization of ZnO nanoparticles coated paper and its antibacterial activity study. Green Chem 8(12):1034–1041. https://doi.org/10.1039/b605623g
9. Garcia MA, Merino JM, Fernández Pinel E, Quesada A, de la Venta J, Ruíz González ML, Castro GR, Crespo P, Llopis J, González-Calbet JM, Hernando A (2007) Magnetic properties of ZnO nanoparticles. Nano Lett 7(6):1489–1494. https://doi.org/10.1021/nl070198m
10. Sajid MM, Shad NA, Javed Y, Shafique M, Afzal AM, Khan SB, Amin N, Hassan MA, Khan MUH, Tarabi T, Zhai H (2022)

Efficient photocatalytic and antimicrobial behaviour of zinc oxide nanoplates prepared by hydrothermal method. J Cluster Sci 33(2):773–783. https://doi.org/10.1007/s10876-021-02013-8
11. Hussain A, Oves M, Alajmi MF, Hussain I, Amir S, Ahmed J, Rehman MT, El-Seedi HR, Ali I (2019) Biogenesis of ZnO nanoparticles using *Pandanus odorifer* leaf extract: anticancer and antimicrobial activities. RSC Adv 9(27):15357–15369. https://doi.org/10.1039/C9RA01659G
12. Pandurangan M, Enkhtaivan G, Kim DH (2016) Anticancer studies of synthesized ZnO nanoparticles against human cervical carcinoma cells. J Photochem Photobiol B 158:206–211. https://doi.org/10.1016/j.jphotobiol.2016.03.002
13. Shaban AS, Owda ME, Basuoni MM, Mousa MA, Radwan AA, Saleh AK (2022) *Punica granatum* peel extract mediated green synthesis of zinc oxide nanoparticles: structure and evaluation of their biological applications. Biomass Conv Bioref. https://doi.org/10.1007/s13399-022-03185-7
14. Shah Mohammad GRK, Seyedi SMR, Karimi E, Homayouni-Tabrizi M (2019) The cytotoxic properties of zinc oxide nanoparticles on the rat liver and spleen, and its anticancer impacts on human liver cancer cell lines. J Biochem Mol Toxicol 33(7):e22324. https://doi.org/10.1002/jbt.22324
15. Majeed S, Danish M, Ismail MHB, Ansari MT, Ibrahim MNM (2019) Anticancer and apoptotic activity of biologically synthesized zinc oxide nanoparticles against human colon cancer HCT-116 cell line- in vitro study. Sustain Chem Pharm 14:100179. https://doi.org/10.1016/j.scp.2019.100179
16. Altalhi TA, Ibrahim MM, Mersal GA, Mahmoud MHH, Kumeria T, El-Desouky MG, El-Bindary AA, El-Bindary MA (2022) Adsorption of doxorubicin hydrochloride onto thermally treated green adsorbent: equilibrium, kinetic and thermodynamic studies. J Mol Struct 1263:133160. https://doi.org/10.1016/j.molstruc.2022.133160
17. El-Bindary MA, El-Desouky MG, El-Bindary AA (2022) Adsorption of industrial dye from aqueous solutions onto thermally treated green adsorbent: a complete batch system evaluation. J Mol Liq 346:117082. https://doi.org/10.1016/j.molliq.2021.117082
18. AlHazmi GA, AbouMelha KS, El-Desouky MG, El-Bindary AA (2022) Effective adsorption of doxorubicin hydrochloride on zirconium metal-organic framework: equilibrium, kinetic and thermodynamic studies. J Mol Struct 1258:132679. https://doi.org/10.1016/j.molstruc.2022.132679
19. Priyadharshini RI, Prasannaraj G, Geetha N, Venkatachalam P (2014) Microwave-mediated extracellular synthesis of metallic silver and zinc oxide nanoparticles using macro-algae (*Gracilaria edulis*) extracts and its anticancer activity against human PC3 cell lines. Appl Biochem Biotechnol 174(8):2777–2790. https://doi.org/10.1007/s12010-014-1225-3
20. Zhang D, Ma XL, Gu Y, Huang H, Zhang GW (2020) Green synthesis of metallic nanoparticles and their potential applications to treat cancer. Front Chem 8:799. https://doi.org/10.3389/fchem.2020.00799
21. Mahdavi S, Afkhami A, Merrikhpour H (2015) Modified ZnO nanoparticles with new modifiers for the removal of heavy metals in water. Clean Technol Environ Policy 17(6):1645–1661. https://doi.org/10.1007/s10098-015-0898-9
22. Salehi-Babarsad F, Derikvand E, Razaz M, Yousefi R, Shirmardi A (2020) Heavy metal removal by using ZnO/organic and ZnO/inorganic nanocomposite heterostructures. Int J Environ Anal Chem 100(6):702–719. https://doi.org/10.1080/03067319.2019.1639685
23. Gu M, Hao L, Wang Y, Li X, Chen Y, Li W, Jiang L (2020) The selective heavy metal ions adsorption of zinc oxide nanoparticles from dental wastewater. Chem Phys 534:110750. https://doi.org/10.1016/j.chemphys.2020.110750
24. Ahmad F, Liu P (2020) (Ascorb)ing Pb neurotoxicity in the developing brain. Antioxidants 9(12):1311. https://doi.org/10.3390/antiox9121311
25. Wu F, Zhang G, Dominy P, Wu H, Bachir DM (2007) Differences in yield components and kernel Cd accumulation in response to Cd toxicity in four barley genotypes. Chemosphere 70(1):83–92. https://doi.org/10.1016/j.chemosphere.2007.06.051
26. Masoud MS, Zidan AA, El Zokm GM, Elsamra RMI, Okbah MA (2022) Humic acid and nano-zeolite NaX as low cost and eco-friendly adsorbents for removal of Pb (II) and Cd (II) from water: characterization, kinetics, isotherms and thermodynamic studies. Biomass Conver Biorefin. https://doi.org/10.1007/s13399-022-02608-9
27. Zhang Y, Zhao M, Cheng Q, Wang C, Li H, Han X, Fan Z, Su G, Pan D, Li Z (2021) Research progress of adsorption and removal of heavy metals by chitosan and its derivatives: a review. Chemosphere 279:130927. https://doi.org/10.1016/j.chemosphere.2021.130927
28. Mahamadi C, Nharingo T (2010) Competitive adsorption of $Pb^{2+}$, $Cd^{2+}$ and $Zn^{2+}$ ions onto *Eichhornia crassipes* in binary and ternary systems. Bioresour Technol 101(3):859–864. https://doi.org/10.1016/j.biortech.2009.08.097
29. Saritha D (2022) A concise review on the removal of heavy metals from wastewater using adsorbents. Mater Today Proc 62:3973–3977. https://doi.org/10.1016/j.matpr.2022.04.579
30. Yang Y, Yue Y, Runwei Y, Guolin Z (2010) Cytotoxic, apoptotic and antioxidant activity of the essential oil of *Amomum tsao-ko*. Bioresour Technol 101(11):4205–4211. https://doi.org/10.1016/j.biortech.2009.12.131
31. Bagur H, Poojari CC, Melappa G, Rangappa R, Chandrasekhar N, Somu P (2020) Biogenically synthesized silver nanoparticles using endophyte fungal extract of *Ocimum tenuiflorum* and evaluation of biomedical properties. J Cluster Sci 31(6):1241–1255. https://doi.org/10.1007/s10876-019-01731-4
32. Dulta K, Koşarsoy Ağçeli G, Chauhan P, Jasrotia R, Chauhan PK (2021) A novel approach of synthesis zinc oxide nanoparticles by bergenia ciliata rhizome extract: antibacterial and anticancer potential. J Inorg Organomet Polym Mater 31(1):180–190. https://doi.org/10.1007/s10904-020-01684-6
33. Yin X, Meng X, Zhang Y, Zhang W, Sun H, Lessl JT, Wang N (2018) Removal of V (V) and Pb (II) by nanosized TiO2 and ZnO from aqueous solution. Ecotoxicol Environ Saf 164:510–519. https://doi.org/10.1016/j.ecoenv.2018.08.066
34. Maensiri S, Laokul P, Promarak V (2006) Synthesis and optical properties of nanocrystalline ZnO powders by a simple method using zinc acetate dihydrate and poly(vinyl pyrrolidone). J Cryst Growth 289(1):102–106. https://doi.org/10.1016/j.jcrysgro.2005.10.145
35. Rahaiee S, Ranjbar M, Azizi H, Govahi M, Zare M (2020) Green synthesis, characterization, and biological activities of saffron leaf extract-mediated zinc oxide nanoparticles: a sustainable approach to reuse an agricultural waste. Appl Organomet Chem 34(8):e5705. https://doi.org/10.1002/aoc.5705
36. Mahdi Z, Yu QJ, El Hanandeh A (2018) Removal of lead(II) from aqueous solution using date seed-derived biochar: batch and column studies. Appl Water Sci 8(181):1. https://doi.org/10.1007/s13201-018-0829-0
37. El-Belely EF, Farag MM, Said HA, Amin AS, Azab E, Gobouri AA, Fouda A (2021) Green synthesis of zinc oxide nanoparticles (ZnO-NPs) using *Arthrospira platensis* (Class: Cyanophyceae) and evaluation of their biomedical activities. Nanomaterials 11(1):95. https://doi.org/10.3390/nano11010095
38. Huang C, Huang CP, Morehart AL (1991) Proton competition in Cu(II) adsorption by fungal mycelia. Water Res 25(11):1365–1375. https://doi.org/10.1016/0043-1354(91)90115-7
39. Alswata AA, Ahmad MB, Al-Hada NM, Kamari HM, Hussein MZB, Ibrahim NA (2017) Preparation of zeolite/zinc

oxide nanocomposites for toxic metals removal from water. Results Phys 7:723–731. https://doi.org/10.1016/j.rinp.2017.01.036
40. Hu X, Qiao Y, Wang B, Hou Y, Zheng F, Li Q (2019) Efficient $Pb^{2+}$ adsorption of biomorphic porous ZnO derived from legume straw. Environ Prog Sustain Energy 38(5):13191. https://doi.org/10.1002/ep.13191
41. Wu J, Wang T, Shi N, Min F, Pan WP (2022) Hierarchically porous biochar templated by in situ formed ZnO for rapid $Pb^{2+}$ and $Cd^{2+}$ adsorption in wastewater: experiment and molecular dynamics study. Environ Pollut 302:119107. https://doi.org/10.1016/j.envpol.2022.119107
42. Zhang BL, Qiu W, Wang PP, Liu YL, Zou J, Wang L, Ma J (2020) Mechanism study about the adsorption of Pb(II) and Cd(II) with iron-trimesic metal-organic frameworks. Chem Eng J 385:123507. https://doi.org/10.1016/j.cej.2019.123507
43. Lanjwani MF, Khuhawar MY, Khuhawar TMJ, Lanjwani AH, Memon SQ, Soomro WA, Rind IK (2022) Photocatalytic degradation of eriochrome black T dye by ZnO nanoparticles using multivariate factorial, kinetics and isotherm models. J Cluster Sci 18:1–2. https://doi.org/10.1007/s10876-022-02293-8
44. Sharifpour E, Ghaedi M, Nasiri Azad F, Dashtian K, Hadadi H, Purkait MK (2018) Zinc oxide nanorod-loaded activated carbon for ultrasound-assisted adsorption of safranin O: central composite design and genetic algorithm optimization. Appl Organomet Chem 32(2):e4099. https://doi.org/10.1002/aoc.4099
45. Torab-Mostaedi M, Asadollahzadeh M, Hemmati A, Khosravi A (2015) Biosorption of lanthanum and cerium from aqueous solutions by grapefruit peel: equilibrium, kinetic and thermodynamic studies. Res Chem Intermed 41(2):559–573. https://doi.org/10.1007/s11164-013-1210-4
46. Taha AA, Shreadah MA, Ahmed AM, Heiba HF (2016) Multi-component adsorption of Pb(II), Cd(II), and Ni(II) onto Egyptian Na-activated bentonite; equilibrium, kinetics, thermodynamics, and application for seawater desalination. J Environ Chem Eng 4(1):1166–1180. https://doi.org/10.1016/j.jece.2016.01.025
47. Liu J, Wang X (2013) Novel silica-based hybrid adsorbents: lead(II) adsorption isotherms. Sci World J 897159. https://doi.org/10.1155/2013/897159
48. Saruchi SM, Hatshan MR, Kumar V, Rana A (2020) Sequestration of eosin dye by magnesium (II)-doped zinc oxide nanoparticles: its kinetic, isotherm, and thermodynamic studies. J Chem Eng Data 66(1):646–657. https://doi.org/10.1021/acs.jced.0c00810
49. Kausar A, Bhatti HN, MacKinnon G (2013) Equilibrium, kinetic and thermodynamic studies on the removal of U(VI) by low cost agricultural waste. Colloids Surf B Biointerfaces 111:124–133. https://doi.org/10.1016/j.colsurfb.2013.05.028
50 El-Enein SA, Okbah MA, Hussain SG, Soliman NF, Ghounam HH (2020) Adsorption of selected metals ions in solution using nano-bentonite particles: isotherms and kinetics. Environ Process 7:463–477. https://doi.org/10.1007/s40710-020-00430-x
51. Yu F, Li Y, Huang G, Yang C, Chen C, Zhou T, Zhao Y, Ma J (2020) Adsorption behavior of the antibiotic levofloxacin on microplastics in the presence of different heavy metals in an aqueous solution. Chemosphere 260:127650. https://doi.org/10.1016/j.chemosphere.2020.127650
52. Premanathan M, Karthikeyan K, Jeyasubramanian K, Manivannan G (2011) Selective toxicity of ZnO nanoparticles toward Gram-positive bacteria and cancer cells by apoptosis through lipid peroxidation. Nanomedicine 7(2):184–192. https://doi.org/10.1016/j.nano.2010.10.001
53. Sivakumar P, Lee M, Kim YS, Shim MS (2018) Photo-triggered antibacterial and anticancer activities of zinc oxide nanoparticles. J Mater Chem B Mater Biol Med 6(30):4852–4871. https://doi.org/10.1039/C8TB00948A
54. Rana SV (2008) Metals and apoptosis: recent developments. J Trace Elem Med Biol 22(4):262–284. https://doi.org/10.1016/j.jtemb.2008.08.002
55. Murphy EA, Majeti BK, Barnes LA, Makale M, Weis SM, Lutu-Fuga K, Wrasidlo W, Cheresh DA (2008) Nanoparticle-mediated drug delivery to tumor vasculature suppresses metastasis. Proc Natl Acad Sci USA 105(27):9343–9348. https://doi.org/10.1073/pnas.0803728105

**Publisher's note** Springer Nature remains neutral with regard to jurisdictional claims in published maps and institutional affiliations.